

A SURVEY OF MEDICAL IMAGE REGISTRATION ON MULTI-CORE AND GPU

Ramtin Shams¹, Parastoo Sadeghi¹, Rodney A. Kennedy¹, and Richard I. Hartley^{1,2}

¹Research School of Information Sciences and Engineering (RSISE),
The Australian National University (ANU)

² National ICT Australia (NICTA)*

1. IN AN OPERATING ROOM NOT SO FAR INTO THE FUTURE

A surgeon is performing a potentially life-saving *pancreatectomy* on a patient in early stages of pancreatic cancer. Two small incisions of no more than half an inch allow *laparoscopic* tools including a video camera and an ultrasound probe to be guided inside the abdominal cavity. A third, larger incision, is occupied by a hand-access device that facilitates the operation. The surgeon is able to locate the tumor in the ultrasound view with ease. This is largely possible due to a newly installed 3D navigation and visualization system that virtually renders the patient transparent.

The visualization system combines data from preoperative magnetic resonance (MR) and computed tomography (CT) scans with intraoperative laparoscopic ultrasound data to produce real-time high quality and dynamic 3D images of the patient, in a process better known as *multi-modal registration* and *fusion*. The high quality 3D images of the tumor and the surrounding tissue allow the surgeon to resect the malignant cells with little damage to healthy structures.

Such a minimally invasive approach avoids the trauma of open surgery, and a faster recovery time means that the patient will be released from the hospital in just two days.

2. MULTIPROCESSING IN AN OPERATING ROOM

Image-guided therapy (IGT) systems play an increasingly important role in clinical treatment and interventions. By providing more accurate information about a patient during a procedure, these systems improve the quality and accuracy of procedures and make less invasive options for treatment available. They contribute to reduced morbidity rate, intervention time, post-intervention care, and procedure costs. For practical reasons, however, imaging systems that can be deployed in an operating room produce images with lower resolutions and signal to noise ratios than can be achieved by the state-of-the-art imaging systems preoperatively. Therefore, it is desirable to be able to use preoperative images of a patient

together with those acquired during a procedure for best results. In brain surgery, for example, the main challenge is to remove as much as the malignant tissue as possible without affecting critical structures and while minimizing damage to healthy tissue. The surgeon uses high quality CT and MR scans of the patient to carefully plan a procedure. During a procedure, however, the brain undergoes varying levels of deformations at different stages of the surgery known as the *brain shift*. This brain shift, a result of change in the intracranial pressure, leakage of cerebrospinal fluid and removal of tissue, affects the accuracy of earlier planning and needs to be compensated for. The surgeon may take a number of intraoperative scans to correct the plan based on patient's current state and also to detect complications such as bleeding. To support the surgeon, the IGT system needs to register intraoperative scans with the patient and with preoperative images.

Modern medical imaging technologies are capable of producing high resolution 3D or 4D (3D + time) images. This makes medical image processing tasks at least one dimension more compute-intensive than standard 2D image processing applications. The higher computational cost of medical image analysis together with the time constraints imposed by the medical procedure determine the range of tools that can be practically offered through an IGT platform. It also often means that an IGT platform has to rely on high performance computing (HPC) hardware and highly parallelized software. There are other practical considerations. For example, equipment used in an operating room should be designed to minimize footprint, power consumption, operating noise, and cost.

The continued development of multi-core and massively multiprocessing architectures in recent years holds great promise for interventional setups. In particular, massively multiprocessing graphics units with general purpose programming capabilities have emerged as front runners for low cost high performance processing. HPC, in the order of 1 TFLOPS, is available on commodity single-chip GPUs with power requirements not much greater than an office computer. Multi-GPU systems with up to 8 GPUs can be built in a single host and can provide a nominal processing capacity of 8 TFLOPS with less than 1500W power consumption under full load.

Hardware and architectural complexities in designing

*NICTA is a research centre funded by the Australian Government through Backing Australia's Ability and the ICT Research Centre of Excellence programs.

multi-core systems aside, perhaps as big a challenge is an overhaul of existing application design methodologies to allow efficient implementation on a range of massively multi-core architectures. As one quickly might find, direct adaptation of existing serial algorithms is more often than not neither possible due to hardware constraints nor computationally justified.

In this paper, we look at previous, recent, and state-of-the-art methods for registration of medical images using a range of HPC architectures including symmetric multiprocessing (SMP), massively multiprocessing (MMP) and architectures with distributed memory (DM) and non-uniform memory access (NUMA). The paper is designed to be self-sufficient. We will take the time to define and describe concepts of interest, albeit briefly, in the context of image registration and high performance computing. We provide an overview of the registration problem and its main components in Section 3. Our main focus will be HPC-related aspects and we will highlight relevant issues as we explore the problem domain. This approach presents a fresh angle on the subject than previously investigated by the more general and classic reviews in the literature [1, 2, 3]. Section 4 and Section 5 are organized from the perspective of high performance and parallel computing with the registration problem embodied. This is meant to equip the reader with the knowledge to map a registration problem to a given computing architecture. Finally, we have endeavored to provide a comprehensive summary of existing contributions from various groups in Section 6.

3. REGISTRATION

Registration is a fundamental task frequently encountered in image processing applications [1]. In medical applications, images of similar or differing *modalities* often need to be aligned as a preprocessing step for many planning, navigation, data-fusion and visualization tasks. Registration of images has been extensively researched in the medical imaging domain. Image based registration may use features that are derived from the subject’s anatomy or those artificially introduced specifically for registration purposes. The former class of registration methods are known as *intrinsic* and the latter as *extrinsic* [2]. Extrinsic methods involve introduction of foreign objects such as stereotactic frames or fiducial markers and may be invasive. Once attached to the subject, markers remain fixed for multiple imaging sessions and can be used to align the images. Intrinsic methods, on the other hand, are non-invasive and can be used retrospectively. They may match a small set of corresponding anatomical and geometrical *landmarks*, use a set of structures obtained through *segmentation*, or be based on the entire content of images (e.g. voxel intensities). Content-based methods are particularly of interest since they can be fully automated but are typically compute-intensive. The focus of this survey is content-based registration methods.

Fig. 1 shows various components of a general registration solver, with the main components being a *transformer*, a *measure*, and an *optimizer*. Registration as depicted here is an iterative process where one image is transformed within a pre-determined parameter space and compared against the other. We call the former the *moving* and the latter the *fixed* image. A measure of similarity or distance is computed between the images at each step and used to determine if they are ‘sufficiently’ aligned. This process is controlled by the optimizer which starts from an initial guess and determines subsequent steps in order to reach an optimal alignment. We will discuss each component in more detail in the following subsections.

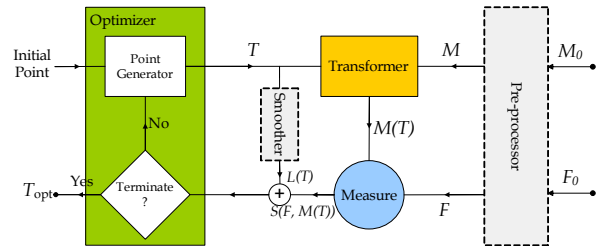


Fig. 1. A general registration solver and its main components: F , M , and $M(T)$ are fixed, moving and transformed moving images, respectively.

3.1. Transformer

The transformer maps points in the moving image to new locations in the transformed image. Depending on the registration problem, a transformation can be *collinear* or *deformable*. Collinear transformations are line-preserving i.e. map straight lines onto straight lines. Collinear transformations can be described by a 4×4 matrix acting on homogeneous vectors representing 3D points. Examples of collinear transformations include *rigid*, *similarity*, *affine*, and *projective*¹. For this reason, these types of transformations have nearly identical complexity. Methods that implement rigid registration can be easily extended to affine, often without any change to the transformer.

Deformable transformation methods can be further categorized as *parametric* and *non-parametric*. Non-parametric methods are based on a *variational* formulation of the registration problem, where the transformation is described by an arbitrary displacement field *regularized* by some smoothing criteria [4]. Parametric methods are based on some piecewise polynomial interpolation of a displacement field using a set of control points placed in the image domain. B-splines are the favorites because they induce local deformations that limit the computational complexity of a large grid of control points [5]. Other functions such as thin-plate splines and Bezier functions have also been used. There are efficient methods

¹Projective transformations are rarely required in medical imaging applications.

168 for non-parametric registration including *multi-grid* solvers.
169 While parametric methods are more demanding, they yield
170 themselves more easily to multi-modal registration applica-
171 tions.

172 The transformer determines the intensity of the points in
173 the transformed image by interpolating intensity values of
174 corresponding points in the moving image. The simplest and
175 fastest interpolation method is the *nearest neighbor* interpo-
176 lation. Nearest neighbor should never be used in practice, as
177 it results in poorly shaped cost functions, but may be use-
178 ful to establish the baseline performance of the transformer.
179 The most commonly used interpolation method is *linear inter-*
180 *polation*. Other methods include *quadratic*, *cubic*, *cubic*
181 *B-spline*, and *Gaussian* interpolation [6].

182 A transformer spends the majority of its time performing
183 interpolations. As noted by Castro-Pareja et al. [7] interpo-
184 lation of the transformed moving image does not benefit from
185 standard memory caching mechanisms due to non-sequential
186 pattern of access to memory with low locality. As a result,
187 transformer performance can well become memory-bound.

188 3.2. Measure

189 A method of measuring the similarity or distance between im-
190 ages is required for automatic registration. Ideally a similarity
191 measure attains its maximum, where the images are perfectly
192 aligned and decreases as the images move farther away. A dis-
193 tance measure, on the other hand, attains its minimum where
194 the images are aligned.

195 Commonly used similarity and distance measures are
196 summarized in Table 1. Just as different classes of transfor-
197 mations are suitable for modeling different geometric distor-
198 tions between the images, different similarity measures are
199 used for different intensity distortions between the images.
200 Measures are broadly categorized based on their suitability
201 for single-modality and multi-modality problems. All of the
202 single-modality measures listed in Table 1 can be calculated
203 by independent computations at each spatial location. From a
204 parallelization point of view, this makes them readily adapt-
205 able to single instruction multiple data (SIMD) instruction
206 sets and architectures such as GPUs. Multi-modality mea-
207 sures determine statistical (mutual information) or functional
208 (correlation ratio) dependance of images where each image
209 is assumed to be a realization of an underlying discrete ran-
210 dom variable. These methods require estimation of joint and
211 marginal probability mass functions (pmfs) of the underlying
212 discrete random variables from image data. Methods of pmf
213 computation can be parallelized with varying degrees of dif-
214 ficulty and performance improvement. We will discuss this
215 issue in more detail in the context of MI computation on the
216 GPU in Section 5.1.

217 3.3. Optimizer

218 The optimizer is responsible for an efficient and often non-
219 exhaustive strategy to search the transformation parameter
220 space for the best match between the images. In image reg-
221 istration, optimizers can be broadly categorized as *gradient-*
222 *based* or *gradient-free*, *global* or *local*, and *serial* or *paral-*
223 *lelizable*.

224 Gradient-based methods require computation of partial
225 derivatives of a cost function in addition to frequent computa-
226 tion of the cost function itself. Therefore, from an implemen-
227 tation perspective, they are more involved than gradient-free
228 methods. The gradient computation can be based on the nu-
229 merical estimation of the derivatives using finite differences.
230 Alternatively, direct computation of the gradient can be per-
231 formed when closed-form equations for the partial derivatives
232 can be derived.

233 Local methods find a local optimum in the vicinity of an
234 initial point and within their *capture range*. They may con-
235 verge to an incorrect alignment if not properly initialized.
236 Global methods, however, find the global optimum within a
237 given range of parameters. They are robust with respect to
238 selection of the initial point but at the cost of slower conver-
239 gence. Global and local methods may be combined to im-
240 prove robustness while maintaining a reasonable convergence
241 rate.

242 Some optimization algorithms are only suited for serial
243 execution, where each optimization step is dependent on the
244 outcome of previous step(s). Others may be amenable to par-
245 allelization. For example, each step of the gradient descent
246 optimization in N -dimensional space requires computation
247 of N partial derivatives of the cost function. Here, there is
248 limited opportunity to run up to N tasks in parallel, and of
249 course the additional line minimization step that may follow
250 cannot be readily parallelized. We call such methods partially
251 parallelizable. And finally, we refer to optimization methods
252 that have been designed for parallel execution with minimal
253 inter-step dependency as fully parallelizable.

254 Table 2 lists some optimization algorithms used for image
255 registration and their respective classification.

256 The overall performance of a registration algorithm is de-
257 pendent on the effectiveness of the optimization strategy. This
258 in turn depends on the *iterations* needed for the algorithm to
259 converge. For gradient-free optimization, we define an iter-
260 ation as a step which involves a single computation of the
261 cost function. For gradient-based optimization, an iteration is
262 defined as a step that involves a single computation of the gra-
263 dient. Depending on the type of gradient-based method this
264 may involve several evaluations of the cost function.

265 Gradient-based optimizers do more in a single iteration
266 and they also converge with a significantly lower number of
267 iterations compared to gradient-free methods. The conver-
268 gence rate of an optimizer depends on many factors including
269 the size of the parameter space, optimizer settings (e.g. con-

Table 1. Commonly used measures

Measure	Acronym	Type	Usage	Formula ¹
Sum of squared differences	SSD	dist.	single-mod.	$\mathcal{D}_{\text{SSD}}(\mathcal{I}, \mathcal{J}) = \sum_{\mathbf{x} \in \Omega} (\mathcal{I}(\mathbf{x}) - \mathcal{J}(\mathbf{x}))^2$
Sum of absolute differences	SAD	dist.	single-mod.	$\mathcal{D}_{\text{SAD}}(\mathcal{I}, \mathcal{J}) = \sum_{\mathbf{x} \in \Omega} \mathcal{I}(\mathbf{x}) - \mathcal{J}(\mathbf{x}) $
Normalized cross correlation [1]	NCC	sim.	single-mod.	$\mathcal{S}_{\text{NCC}}(\mathcal{I}, \mathcal{J}) = \sum_{\mathbf{x} \in \Omega} \frac{\mathcal{I}(\mathbf{x})\mathcal{J}(\mathbf{x})}{\sqrt{\mathbb{E}[\mathcal{I}(\mathbf{x})^2]\mathbb{E}[\mathcal{J}(\mathbf{x})^2]}}$
Correlation coefficient [1]	CC	sim.	single-mod.	$\mathcal{S}_{\text{CC}}(\mathcal{I}, \mathcal{J}) = \sum_{\mathbf{x} \in \Omega} \frac{(\mathcal{I}(\mathbf{x}) - \mathbb{E}[\mathcal{I}(\mathbf{x})])(\mathcal{J}(\mathbf{x}) - \mathbb{E}[\mathcal{J}(\mathbf{x})])}{\sigma(\mathcal{I})\sigma(\mathcal{J})}$
Gradient correlation	GC	sim.	single-mod.	$\mathcal{S}_{\text{GC}}(\mathcal{I}, \mathcal{J}) = \frac{1}{d} \sum_{i=1}^d \mathcal{S}_{\text{CC}}\left(\frac{\partial \mathcal{I}}{\partial x_i}, \frac{\partial \mathcal{J}}{\partial x_i}\right)$
Mutual information [8, 9]	MI	sim.	multi-mod.	$\mathcal{S}_{\text{MI}}(\mathcal{I}, \mathcal{J}) = \sum_i \sum_j p_{\mathcal{I}\mathcal{J}}(i, j) \log \frac{p_{\mathcal{I}\mathcal{J}}(i, j)}{p_{\mathcal{I}}(i)p_{\mathcal{J}}(j)}$
Normalized mutual info. [10]	NMI	sim.	multi-mod.	$\mathcal{S}_{\text{NMI}}(\mathcal{I}, \mathcal{J}) = \frac{2\mathcal{S}_{\text{MI}}(\mathcal{I}, \mathcal{J})}{H(\mathcal{I}) + H(\mathcal{J})}$ (see note 2)
Correlation ratio [11]	CR	sim.	multi-mod.	$\mathcal{S}_{\text{CR}}(\mathcal{I}, \mathcal{J}) = \frac{\sigma^2(\mathbb{E}[\mathcal{J} \mathcal{I}])}{\sigma^2(\mathcal{I})}$

¹: $\Omega \subset \mathbb{R}^d$ represents a d -dimensional image domain.

²: Entropy is defined as $H(\mathcal{I}) = \sum_i p_{\mathcal{I}}(i) \log \frac{1}{p_{\mathcal{I}}(i)}$, where image \mathcal{I} is assumed to be a discrete random variable with a probability mass function (pmf) given by $p_{\mathcal{I}}(\cdot)$.

Table 2. Classification of some optimization methods

Method	Classification		
Powell [12]	gradient-free	local	serial
Simplex [13]	gradient-free	local	partially parallelizable
Soblex ¹ [14]	gradient-free	combined	partially parallelizable
MDS ^{1,2} [15]	gradient-free	local	partially parallelizable
Gradient descent [12]	gradient-based	local	partially parallelizable
Quasi-Newton [12]	gradient-based	local	partially parallelizable
Levenberg-Marquardt [12]	gradient-based	local	partially parallelizable
Simulated annealing [12]	gradient-free	combined	partially parallelizable
DIRECT ³ [16]	gradient-free	global	fully parallelizable
Genetic [17]	gradient-free	global	fully parallelizable

¹ : a simplex variant, ² : multidirectional search, ³ : dividing rectangles

3.4. Preprocessor

We have shown the preprocessor in dotted lines in Fig. 1 to emphasize that it is an optional component. Preprocessing encapsulates a wide range of tasks that may be performed on images outside the optimization loop and at the beginning of the process. These may include filtering, rectification, gradient computation, pyramid construction, feature detection, etc. An example is given in one of the earlier efforts to parallelize image registration by Warfield et al. [20]. They extract features based on tissue labels given by prior *segmentation* and parallelize a feature-based inter-patient registration method on a cluster of multiprocessor computers. They use the number of mismatching labels (NML) as a measure of distance in their registration algorithm.

Given that preprocessor is not in the critical pass, there is little incentive for parallelizing it. Unless of course the registration process itself is sped up to the point that preprocessing becomes a bottleneck. This is likely to become the case as registration algorithms enter the real-time domain.

3.5. Computational Expense of Image Registration

Image registration in general is computationally expensive and has been largely confined to preoperative applications. The main bottlenecks are typically the transformer and the computation of the measure. Single modality measures such as sum of squared differences (SSD) and correlation coefficient

vergence criteria), and the misalignment between the images.

It is also often data-dependent.

The computational bottleneck of registration is not the optimizer but the computation of the transformation and the measure. Most researchers have focused on *fine-grained* parallelization of these components. A few have considered *coarse-grained* parallelization which involves parallelization of the optimizer itself [18, 19].

cient² (CC) are less compute-intensive than multi-modality measures such as mutual information (MI) and correlation ratio (CR). Computation of MI requires an estimation of the joint probability density of image intensities. This typically entails, computing a joint histogram of image intensities. A seemingly simple task which is far from trivial on some massively-parallel architectures such as GPUs [22].

A sample breakdown of computations in one iteration of a gradient-free optimization algorithm is given in Table 3 for affine registrations using a single modality and a multi-modality measure. The measurements are based on a Quad core Intel Core i7 920 and an NVIDIA GTX 295. The time spent outside of the measure and transformation components is negligible compared to the measure and transformation. On the CPU the execution time is dominated by the transformer whereas on the GPU, the time spent in computing the measure, particularly for the MI, exceeds the transformer time. This is expected as GPUs are designed to speed up geometric transformations. Obviously, for more complex transformation models such as the deformable B-splines more time will be spent in the transformer for both platforms.

Table 3. A sample breakdown of computations for affine registrations on a multi-core CPU and a GPU

	Affine (SSD)		Affine (MI)	
	Measure	Transform	Measure	Transform
CPU	4.3%	95.7%	13.5%	86.5%
GPU	50.4%	49.2%	86.9%	13.0%

We note that optimization algorithms make decisions based on the measure and do not directly use the intermediate results of the transformer. As such, transformation and similarity measure computations may be performed in one step and within the same module to remove the need for storage and subsequent retrieval of transformed image data. This obviously improves performance, especially where IO traffic is an issue. However, it also makes it more difficult to modularize the implementation and cater for arbitrary combinations of transformations and measures.

4. MULTI-CPU IMPLEMENTATIONS

4.1. Symmetric Multiprocessing

In symmetric multiprocessing (SMP) architectures multiple CPUs/cores have access to a single shared main memory. This makes parallelization of serial code relatively straightforward. The main methods for parallelization on SMP architectures

²Some authors use normalized cross correlation to refer to correlation coefficient. We prefer correlation coefficient which is the accepted term in statistics.

are *POSIX threads* (pthreads) and *OpenMP* [23, 24]. The pthreads standard defines an application programming interface (API) for explicit instantiation, management and synchronization of multiple threads, whereas OpenMP mainly consists of a set of compiler directives (and a supporting API) that allows for implicit parallelization.

Most serial programs can be parallelized on SMP architectures with minimal modification. The ease with which parallelization can be achieved, especially with OpenMP, can be deceiving. There is an adage in HPC circles that ‘OpenMP does not make parallel programming easy, it only makes bad parallel programming easy’. We should emphasize that there is nothing inherently inhibiting about OpenMP or SMP platforms. It is only that optimal parallelization usually requires a change in the algorithm, programming model and memory access pattern in addition to the syntax. We encourage the reader to be prepared to reevaluate the approach to solving a problem on parallel systems and avoid the temptation of simply mapping a serial code to multiple threads. We also advise that use of *synchronization* primitives³ should be limited to a minimum and alternative methods to achieve an outcome without synchronization should be investigated.

A good example of SMP parallelization of a registration algorithm is given by Rohlfing et al. [25]. They use pthreads to parallelize B-spline deformable registration on 64 CPUs. They exploit a combination of procedural (pre-computation, multi-resolution, adaptive activation of control points) and architectural elements (e.g. data partitioning) to optimize their method. While the hardware has been long superseded, their approach is still relevant today. We would not change much about their method except that they use synchronized reduction of partial joint histograms into a global histogram in the MI computation phase by using the *mutex* lock. One can avoid the need for synchronization by dividing partial histograms and the resulting global histogram among the available threads. For N threads, this divides each partial histogram into N equally sized non-overlapping regions. Each thread, then, computes part of the global histogram by summing values across corresponding regions of partial histograms. Since the regions are non-overlapping, the computations are guaranteed to be free of write-conflicts and no synchronization is required.

4.2. Multiprocessing with Non-Uniform Memory Access

Efficient memory access is an important design consideration in multiprocessor systems with many cores where maintaining an efficient cache coherency on a single-shared-bus becomes less practical as the number of processors increases. Non-uniform memory access (NUMA) architecture divides

³Synchronization refers to any mechanism for coordinating multiple threads or processes to complete a task. Examples of synchronization primitives include mutual exclusion (*mutex*), *thread-join*, and *barrier*. Atomic operations also involve implicit synchronization.

388 memory into multiple banks; each assigned to one processor.
 389 Processors have faster access to their local bank than remote
 390 banks attached to other processors.

391 Access to memory on remote banks can be several times
 392 slower than access to local memory. This is due to data trav-
 393 eling through a longer path and also transient access requests
 394 by other processors that may require the memory bus to be
 395 shared. Fig. 2 shows schematic of a multiprocessor system
 396 with a NUMA architecture. An algorithm which is optimally
 397 designed for NUMA makes only infrequent attempts to access
 398 data on remote banks. A parallel application can theoretically
 399 achieve linear scalability with respect to memory throughput
 400 whenever proper distribution of memory to local banks is pos-
 401 sible.

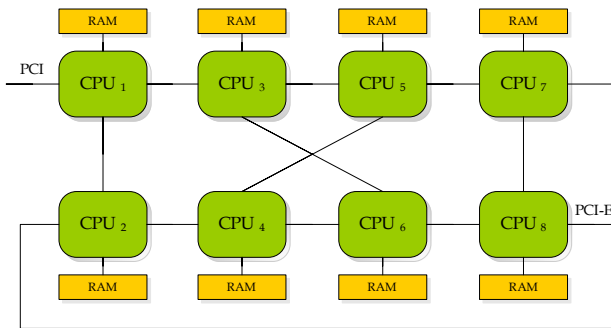


Fig. 2. SunFire X4600 M2 schematic with 8 NUMA nodes. A CPU can access remote memory through a maximum of 3 hops.

402 Image registration can be efficiently implemented on
 403 NUMA architectures as shown in Fig. 3. Both the transform
 404 and measure computation can work on a spatial subset of the
 405 images. To achieve optimal performance, the fixed image F
 406 is divided among the memory banks and the corresponding
 407 portion of the transformed moving image $M(T)$ will also be
 408 stored on the same memory bank. However, the path taken by
 409 the optimization algorithm cannot be determined a priori and
 410 the transformer will use different areas of M to create the lo-
 411 cal portion of $M(T)$ at each iteration. As such, each memory
 412 bank will need to receive a local copy of the moving image
 413 M during the initialization step. Given that the optimization
 414 algorithm will take several iterations to converge, this initial
 415 overhead is justified.

416 The distribution of resources to specific memory banks re-
 417 quires setting an appropriate memory and processor *affinity*⁴.
 418 This is operating system dependent and will make the code
 419 less portable. The alternative is, of course, to be completely
 420 oblivious to the memory architecture and hope that the com-
 421 piler and the operating system will make the right decisions.
 422 This may not be an entirely unreasonable strategy depend-

⁴Processor affinity refers to explicit binding of a thread to a specific pro-
 cessor. Memory affinity is explicit allocation of data on a specific memory
 bank.

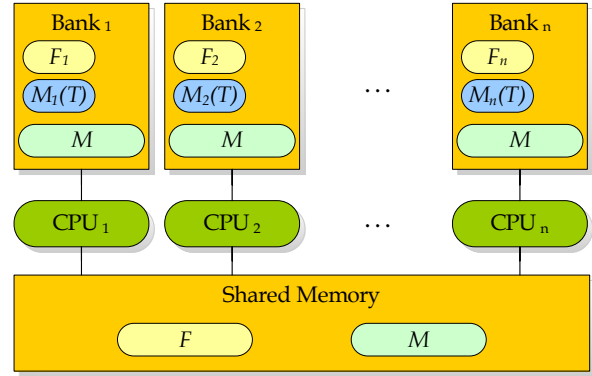


Fig. 3. Partitioning of the data-set among multiple memory banks for improved access. The original data is loaded from a shared storage medium.

423 ing on the number of processors and whether a program is
 424 memory-bound or CPU-bound. However, as the number of
 425 available CPUs increases or for programs that are memory-
 426 intensive, it becomes more important to design an optimal
 427 memory access strategy.

4.3. Multiprocessing with Distributed Memory

428 Distributed memory (DM) architectures are characterized by
 429 lack of access to a global shared memory available to all pro-
 430 cessors. DM systems are typically built by clustering SMP
 431 or NUMA nodes. As such, in distributed architectures, sub-
 432 groups of processors have access to shared memory.
 433

434 From a programming standpoint, these systems are char-
 435 acterized by the need for explicit data distribution and inter-
 436 process communication. The former has to be built into the
 437 application design and the latter is most commonly achieved
 438 through the *message passing interface* (MPI) [26].

439 The model given for data distribution in NUMA Fig. 3 can
 440 be equally applied here. An early implementation is given
 441 by Butz and Thiran [18], where a Linux cluster was used to
 442 speed up MI-based registration for a global genetic optimizer.
 443 In [27], Ino et al. further partition the moving image in order
 444 to reduce the memory usage. This is motivated by the need to
 445 process large images in the order of $1024 \times 1024 \times 590$ voxels.
 446 Partitioning both images also reduces traffic on the network
 447 during initialization. This can be an important consideration
 448 as the number of nodes increases and the overhead of the ini-
 449 tialization phase compared to the optimization phase can no
 450 longer be ignored. Partitioning the moving image requires a
 451 prior estimate of the range of transformation parameters to
 452 ensure that a large enough portion of the image is loaded for
 453 the transformer.

454 A variation is given by *distributed shared memory* (DSM)
 455 architectures, where a large virtual address space is made
 456 available to all processes across all nodes. DSM can only
 457 hide the mechanism of communication between processes

458 and not the associated latency. We argue that if the end goal
459 is to achieve the highest performance, little benefit can be
460 drawn from the convenience of a DSM architecture and the
461 program should be designed to be aware of the locality of
462 data.

463 Wachowiak and Peters [19] develop MI-based registra-
464 tion for a DSM architecture. Their implementation does not
465 take memory locality into account but they use DIRECT
466 and MDS parallel optimization methods to their advan-
467 tage. This coarse-grained parallelization results in lower
468 communication-to-computation overhead.

469 As some authors have pointed out [28], a major benefit of
470 DM clusters is their lower cost compared to many-core SMPs
471 or DSM systems.

472 5. ACCELERATOR IMPLEMENTATIONS

473 5.1. Graphics Processing Unit (GPU)

474 The majority of recent research in multi-core adaptation of
475 registration algorithms has been focused on GPUs [29, 30, 31,
476 32, 33, 34, 35]. There are several reasons for the interest in
477 GPUs. Thanks to fierce competition and driven by the gam-
478 ing industry, GPUs today provide some of the highest per-
479 formance per dollar and the lowest power consumption per
480 FLOPS of any computing platform. While, not every radi-
481 ology department can afford the cost and space needed by a
482 conventional HPC data-center, they can certainly benefit from
483 unlocking the computational power of the GPUs in their ex-
484 isting computers.

485 GPU implementations tend to be more challenging than
486 multi-core CPU implementations and are more rewarding in
487 terms of achievable performance gains. Earlier work in this
488 area (mainly prior to 2007) [36, 37, 38, 39, 40, 41, 42, 43]
489 involved devising methods to map the registration problem
490 onto a *graphics pipeline* which was not specifically designed
491 for general purpose computing. The GPU landscape has since
492 gone through a seismic change with the introduction of na-
493 tive general purpose computing capabilities in late 2006. The
494 GPU registration literature prior to 2007 has been superseded
495 from both hardware and software perspectives. We will fo-
496 cus on the latest technology for general purpose computing
497 on GPUs in this section.

498 The modern software platforms for general purpose pro-
499 gramming on the GPU are currently NVIDIA's CUDA [44]
500 and AMD/ATI's Brook+ [45]. These platforms are vendor-
501 specific, however OpenCL compliant implementations that
502 provide hardware-independence are being gradually released
503 by the vendors. This essentially invalidates the only remain-
504 ing argument in favor of using the graphics pipeline for gen-
505 eral purpose programming, which has been better portability.

506 None of the papers we considered for this survey devel-
507 oped their methods for ATI Brook+. It appears that the re-
508 search community has almost exclusively adopted CUDA as

509 their preferred GPU platform. This is likely to change with
510 wider support for OpenCL in non-GPU architectures such as
511 IBM's Cell/BE and Intel's Larrabee.

512 Modern GPUs extend the *single instruction multiple data*
513 (SIMD) paradigm to a *single instruction multiple threads*
514 architecture (SIMT). SIMT provides more flexibility by par-
515 allelism for (almost) independent threads as well as data-
516 parallel code. GPUs achieve their computational perfor-
517 mance by dedicating more transistors to their arithmetic
518 logic units (ALUs) for data processing, at the expense of
519 reduced flow control and data caching. They extend the
520 conventional *thread-level* parallelism by introducing two
521 additional layers of parallelism in the form of closely knit
522 groups of threads known as *warps* or *wavefronts*, and groups
523 of warps/wavefronts known as *thread blocks* or simply *blocks*.
524 Warps are significant since they define the unit of flow control
525 in a GPU. Threads in a warp are bound to execute the same
526 instruction (on different data). Diverging paths of execution
527 for threads in a warp result in serial execution of all paths.
528 Hence, an important consideration in adapting parallel code
529 to GPU architecture is minimizing diversion in warps. This
530 can be achieved by designing *warp-aware* algorithms and
531 reorganizing data to optimize flow control. An example of
532 such an approach is given in [34].

533 Another notable technical feature in the current gener-
534 ation of GPUs is the availability of an abundance of high
535 bandwidth on-board RAM. The memory bandwidth of top-
536 of-the-line GPUs exceeds 140GB/s and cards with up to 4GB
537 of memory are available. This is particularly important for
538 medical image analysis applications that have to deal with
539 large 3D data-sets. Despite an extremely high bandwidth, the
540 GPU's main memory is largely un-cached and suffers from
541 a rather large latency. Hence to fully utilize the bandwidth
542 and achieve an optimal performance, one needs to understand
543 the hardware architecture and its various memory and limited
544 caching models. Optimum use of memory such as *coalesced*
545 transfers may speed up an application by an order of magni-
546 tude. This level of flexibility is typically available with lower
547 level APIs and runtime SDKs such as CUDA (NVIDIA) [44]
548 and CAL (ATI/AMD) [45]. Programs developed with a lower
549 level API lack portability and need to be maintained as the
550 hardware evolves. Abstraction layers such as OpenCL and
551 Brook+ avoid these issues by hiding memory management
552 details from the developer. However, better portability may
553 come at the cost of sub-optimal performance.

554 GPUs are well equipped for speeding up geometric trans-
555 formations. Geometric transformations (regardless of their
556 type) require some sort of interpolation that involves read-
557 ing the content of adjacent voxels in a cubic region of mem-
558 ory. Standard computer architectures are designed to opti-
559 mize sequential memory access through their caching mech-
560 anism. This does not fully benefit 3D interpolations over a
561 cubic mesh. Modern GPUs, on the other hand, support a 3D
562 texture addressing mode that takes the geometric locality into

563 account for caching purposes. This greatly improves the effi-
564 ciently of transformations on the GPU.

565 Different MI computation methods on the GPU have been
566 reported in the literature. Shams et al. compute MI by com-
567 puting joint histograms on the GPU in [22, 30, 34]. A main
568 finding is that for different sized histograms (number of bins
569 used for MI computation), the optimal algorithm differs. For
570 bin ranges typical in MI computation (100×100 and above)
571 an efficient histogram computation algorithm specifically de-
572 signed for massively multi-processing architectures is pre-
573 sented in [34]. The paper describes a new method for his-
574 togram computation (*sort and count*) that removes the need
575 for synchronization or atomic operations, based on sorting
576 chunks of data with a parallel sort algorithm such as *bitonic*
577 sort. Lin and Medioni [31] report an adaption of Viola’s MI
578 computation approach [8]. Their method approximates the
579 joint pmf by stochastic sampling of the image intensities and
580 using Parzen windowing. This method lends itself well to par-
581 allelization on the GPU, reduces the computational burden of
582 transformations by only using a subset of image data, and pro-
583 vides analytic equations for computation of MI derivatives.
584 However, sparse sampling of the data-set may compromise
585 accuracy of the registration [38]. A sampling method specifi-
586 cally designed for the GPU is given by Shams and Barnes
587 [30]. This method samples the bin space for computing his-
588 tograms rather than the intensity space. The method improves
589 performance of computations and is subject to the same trade
590 off between performance and accuracy. We note that a ma-
591 jority of researchers use direct computation of the histogram
592 [3].

593 A natural extension to parallelization of registration algo-
594 rithms on the GPU is horizontal parallelization across multi-
595 ple GPUs. Multi-GPU systems belong to DM class of parallel
596 architectures. An implementation on such systems involves
597 data partitioning and the use of MPI as discussed in Section
598 4.3. We recommend the reader to refer to a more detailed dis-
599 cussion of the subject in another article in this issue of Signal
600 Processing Magazine by Plishker et al. [46].

601 5.2. Cell Broadband Engine (CELL/BE)

602 Cell/BE is an asymmetric heterogeneous multi-core processor
603 with a distributed memory architecture. It comprises a gen-
604 eral purpose PowerPC core known as a PPE and eight spe-
605 cialized vector processing cores known as SPEs. Each SPE
606 is equipped with a 4-way SIMD engine and has its own small
607 (un-cached) memory known as the local storage⁵.

608 Optimal implementation of registration algorithms on
609 Cell/BE architectures involves task-level parallelization, data
610 partitioning, and vectorization of the code for the SPEs’
611 SIMD engine. It also involves handling the transfer of data
612 between the system memory and SPEs’ local storage. The

⁵Local storage is only 256KB in current generation of hardware and is shared between data and kernel instructions.

613 results by Ohara et al. [47, 48] and Rohrer and Gong [49]
614 provide good insight into challenges involved in designing
615 registration on this architecture for collinear and deformable
616 registration, respectively.

617 5.3. Field Programmable Gate Array (FPGA)

618 A custom FPGA accelerator prototype for MI-based rigid reg-
619 istration is given by Castro-Pareja et al. in [7]. They argue
620 that a major bottleneck in MI computation using Collignon’s
621 method [9] is partial volume (PV) interpolation and that it is
622 memory-bound. They improve performance by parallelizing
623 access to memory and assigning independent memory con-
624 trollers and types of memory for storage and access to the
625 fixed image, the moving image, and the joint histogram. A *cu-
626 bic* addressing scheme is used for the moving image to speed
627 up the interpolation. This is similar to caching available in
628 GPUs for access to texture memory. An enhanced version of
629 [7] is presented in [50] and a multi-rigid version with volume
630 subdivisions is given by Dandekar [51].

631 FPGAs allow one to design customized hardware for spe-
632 cific registration tasks. However, they provide less flexibility
633 compared to software-based implementations. With flexible
634 general purpose programming capabilities of modern GPUs,
635 it is doubtful if FPGA-based implementations present any real
636 benefit in this area.

637 6. SUMMARY OF THE LITERATURE

638 We have summarized existing contributions in high perfor-
639 mance computation of registration methods in Table 4. The
640 table serves as a quick reference to an array of methods on
641 various platforms and by different groups.

642 Researchers have used various methods to present their
643 performance results. All groups report at least the speedup
644 results compared to a single-core CPU implementation. When
645 inter-architecture comparisons are drawn, it is not always
646 clear how well the CPU implementation has been optimized,
647 if the SSE instruction set has been used, whether the code
648 has been compiled as 64- or 32-bit, or if 64- or 32-bit floating
649 point operations have been used. For these reasons, speedup
650 results should be interpreted with caution, more so when the
651 reported speedups are in the order of a hundred times or more.

652 Most groups report their speedups for the entire registra-
653 tion algorithm and for specific data-sets. Comparison of dif-
654 ferent results is further complicated as authors may have im-
655 plemented a multi-resolution scheme to further speed up the
656 process and used different convergence criteria. We have re-
657 ported/estimated the results for the finest resolution in Table
658 4, where possible. As discussed earlier, the execution time is
659 an almost linear function of the number of iterations of the
660 optimization algorithm. Convergence criteria are most com-
661 monly based on the value of the measure and its relative im-
662 provement in a given step of the optimization. A less common

663 approach is to set a fixed number of iterations as the conver- 708
664 gence criterion. We call the former strategy *dynamic conver-* 709
665 *gence* and the latter *static convergence*. Lack of associativity 710
666 for floating point operations have the inevitable consequence 711
667 that the same optimization algorithm operating on the same
668 data-set converges with different number of iterations on dif-
669 ferent architectures when dynamic convergence is employed.
670 Even on the same architecture, compiler optimization of float-
671 ing point operations results in variations. Unless experiments
672 are performed on a large set of images, this skews the perfor-
673 mance results one way or the other.

674 We have given normalized *performance*⁶ results in Table
675 4 where possible. The purpose of normalizing the reported
676 results is to give the reader an indication of the speedups ex-
677 pected from a method without dependence on the size of im-
678 ages involved, convergence criteria, use of a multi-resolution
679 scheme, and to some extent the type of optimization algo-
680 rithm. Normalized results are given in terms of average exe-
681 cution time in milliseconds for a single iteration of the opti-
682 mization algorithm and for processing 1,000,000 voxel pairs
683 (ms/MVoxel/itr).

684 Many authors have used gradient descent as their opti-
685 mization algorithm, largely due to its simple structure and
686 ease of implementation. Once the gradient is computed the
687 optimizer takes a step along the direction of the gradient. The
688 choices include taking a single step in a direction opposite to
689 the gradient where the step size may be adjusted over time,
690 or use of a line minimization algorithms such as Brent's [12].
691 Line minimization usually involves several computations of
692 the cost function alone without its derivatives.

693 When comparing results it is important to identify which
694 variation of the gradient descent is used. We have come across
695 four different implementations.

- 696 • Type A: Closed-form differentiation with a single step
- 697 • Type B: Closed-form differentiation with line mini- 708
698 mization 709
- 699 • Type C: Numeric differentiation with a single step
- 700 • Type D: Numeric differentiation with line minimiza- 710
701 tion. 711

702 Most authors exclude initialization time, including disk
703 IO and loading data from host memory to GPU memory. This
704 is a reasonable practice since initialization time is typically a
705 small fraction of the registration task. Initialization occurs at
706 the beginning of the registration algorithm whereas the opti-
707 mization loop is executed several times.

⁶The word 'performance' is ambiguous in the context of registration. It is sometimes used to refer to the degree of success for a registration algorithm based on accuracy of the registration results. In this article, we use 'performance' in its computational capacity refereing to execution efficiency of the registration algorithm.

Some of the information presented in Table 4 were not im-
mediately available in the original manuscripts and were pro-
vided by the authors of the respective papers. Unless specifi-
cally specified listed methods are for 3D/3D registration.

7. FINAL WORDS

Over the last decade a rich and diverse literature on high
performance computing of medical image registration has
emerged. Research in this area continues to be motivated
by the need to minimize the overhead of image registration
which is used as an integral part of image guided intervention
and image guided therapy systems. The continued research
in this area will also facilitate the adaption of existing preop-
erative tools to real-time intraoperative environments.

From a technical perspective, there has been a gradual
shift away from expensive SMP supercomputers to less ex-
pensive clusters of commodity computers and more recently
inexpensive massively multiprocessing GPUs. This trend has
the potential to lead to more widespread use of medical imag-
ing tools in everyday clinical practice by making them afford-
able outside of research facilities and expensive operating the-
aters.

8. ACKNOWLEDGEMENTS

We would like to thank Prof. Alistair Rendell for making
staff and computational resources available for our experi-
ments. We would also like to thank Mr. Ahmed El Zein and
Mr. Benjamin Murphy for their efforts in porting the original
code to Solaris, Linux and its adaptation to Brook+.

We also thank many authors, whose work we have re-
ferred in this paper, for providing additional information and
for clarification of their results.

9. REFERENCES

- [1] L. G. Brown, "A survey of image registration techniques," *ACM Computing Surveys*, vol. 24, no. 4, pp. 325–376, Dec. 1992.
- [2] J. B. A. Maintz and M. A. Viergever, "A survey of medical image registration," *Med. Image Anal.*, vol. 2, no. 1, pp. 1–36, 1998.
- [3] J. P. W. Pluim, J. B. A. Maintz, and M. A. Viergever, "Mutual-information-based registration of medical images: A survey," *IEEE Trans. on Med. Imaging*, vol. 22, no. 8, pp. 986–1004, Aug. 2003.
- [4] J. Modersitzki, *Numerical Methods for Image Registration*, Oxford University Press, New York, 2004.
- [5] D. Rueckert, L. I. Sonoda, C. Hayes, D. L. G. Hill, M. O. Leach, and D. J. Hawkes, "Nonrigid registration using free-form deformations: Application to breast MR images," *IEEE Trans. on Med. Imaging*, vol. 18, no. 8, pp. 712–721, Aug. 1999.
- [6] T. M. Lehmann, C. Gönner, and K. Spitzer, "Survey: Interpolation methods in medical image processing," *IEEE Trans. on Med. Imaging*, vol. 18, no. 11, pp. 1049–1075, Nov. 1999.
- [7] C. R. Castro-Pareja, J. M. Jagadeesh, and R. Shekhar, "FAIR: a hardware architecture for real-time 3-D image registration," *IEEE Trans. on Info. Technology in Biomedicine*, vol. 7, no. 4, pp. 426–434, Dec. 2003.
- [8] P. Viola and W. M. Wells III, "Alignment by maximization of mutual information," in *Proc. Int. Conf. Computer Vision (ICCV)*, June 1995, pp. 16–23.

Table 4. Summary of high performance image registration methods in the literature

	Transform	Meas.	Optimizer	Hardware	Year	Perf. ¹	Comments	Group	
CPU	Collinear	Simil.	NML	Powell	2 × Sun Ent. 5000 (2 x 8 UltraSparc I 167MHz)	1998	-	SMP cluster, Feature-based	Warfield [20]
		Affine	MI	Genetic	PC Cluster (10 × 2 Pentium III 550MHz)	2001	-	DM, MI is gradient-based	Butz [18]
		Rigid	LLC	?	PC Cluster (10 × 2 Pentium III 933MHz)	2002	-	Block matching with local linear correlation measure (LLC)	Ourselin [28]
		Rigid	MI, NMI	DIRECT, MDS	SGI Altix 3000 (20 Itanium II 1.3 GHz)	2006	-	DMS (NumaFlex)	Wachowiak [19]
		Rigid	MI	Powell	Sun SPARC T5120 (8 x UltraSPARC T2 1.2GHz)	2009	47.7	SMP, Solaris	Shams ²
		Rigid	MI	Powell	Intel Q6600 (Pentium Core 2 Quad 2.4GHz, 4 cores)	2009	15.8	SMP, 64-bit Linux	Shams ²
		Rigid	MI	Powell	Intel Core i7 920 (Quad 2.66GHz, 8 threads)	2009	13.2	SMP, 64-bit Windows Vista	Shams ²
		Rigid	MI	Powell	SunFire X4600 M2 (8 × 2 Opteron 2.6GHz)	2009	10.5	NUMA, 64-bit Linux	Shams ²
	Def.	B-spline	NMI	Grad. desc. (D)	SGI Origin 3800 (128 MPIS 12K)	2003	-	SMP, Max. CPUs used: 64	Rohlfing [25]
		B-spline	NMI	Grad. desc. (D)	PC Cluster (64 x 2 Pentium III 1GHz)	2005	-	DM (Myrinet)	Ino [27]
GPU	Collinear	Rigid	SSD	Simplex	GeForce 6800	2006	98.0	Coded in OpenGL & GLSL	Köhn [52]
		Rigid	SSD	Grad. desc. (B)	GeForce 6800	2006	858	Coded in OpenGL & GLSL	Köhn ³ [52]
		Rigid	GC	?	Quadro FX 1400, FX 3400, GTX 7800	2006	-	2D/3D registration	Ino [39]
		Rigid	Various	Custom	GeForce 6800 GT	2006	-	Various measures (e.g. SSD, CC, GC)	Khamene ³ [38]
		Rigid	Various	ARS + BN	GeForce 7800 GS	2008	-	2D/3D, Various measures (e.g. SSD, CC, GC), Adaptive Random Search + Best Neighbor	Kubias [43]
		Rigid	MI	Simplex	GTX 8800 (16 MP/ 128 cores)	2007	6.17	CUDA 1.0 (no support for 3D textures), MI estimated by bin sampling	Shams [30]
		Rigid	SSD	Simplex	GTX 8800 (16 MP/ 128 cores)	2008	6.05	CUDA 2.0	Plishker ³ [32]
		Affine	MI	Grad. desc. (A)	GTX 8800 (16 MP/ 128 cores)	2008	-	MI estimated by sampling	Lin [31]
		Rigid	MI	Powell	GTX 280 (30 MP/ 240 cores)	2009	4.06	CUDA 2.0, using 3D textures, MI computed using bitonic sort and count	Shams [34]
		Deformable	Bezier	MI	Powell	GeForce3 64MB	2002	-	
	Non-par.		SSD	Grad. desc.	GeForce FX 5800 Ultra	2004	-	2D/2D, Multi-grid solver used	Strzodka [37]
	Non-par.		SSD	Grad. desc. (B)	GeForce 6800	2006	465	Coded in OpenGL & GLSL	Köhn ³ [52]
	Non-par.		MI + KL	Grad. desc. (C)	GTX 7800	2007	2860	Combined MI & Kullback-Leibler measure, Coded in OpenGL & GLSL	Vetter ³ [40]
	Non-par.		MI + KL	Grad. desc. (C)	GTX 8800 Ultra (16 MP/128 cores)	2008	324	Combined MI & Kullback-Leibler measure, Coded in OpenGL & GLSL	Fan ³ [41]
	Demons		SSD	Iterative	Quadro FX 1400	2007	1050	Coded in Cg, Published in 2008	Courty [42]
	Demons		SSD	Iterative	GTX 8800 (12 MP/96 cores)	2007	11.7	Coded in Brook, SSD excluded in performance results	Sharp ³ [29]
	Demons		CC	Iterative	Quadro FX 5600 (16 MP/128 cores)	2008	9.25	CUDA 0.9	Özçelik [33]
	B-spline		SSD	Grad. desc. (C)	GTX 8800 (16 MP/ 128 cores)	2008	3710	CUDA 2.0	Plishker ³ [32]
	Polynom.		MI	Exhaustive	Quadro FX 5600 (16 MP/128 cores)	2009	-	2D/2D, Ultra large 2D images	Ruiz [35]
	Other Accelerators	Collinear	Rigid	MI	N/A	FPGA (2 x Altera 1K100 80MHz)	2003	101	MI partially computed in h/w
Rigid			MI	N/A	FPGA (1 x Altera EP1S40 200MHz)	2004	20.0	MI fully computed in h/w	Pareja [50]
Affine			MI	Grad. desc.	QS20 (2 × Cell/BE.: 2 × 1 PPE & 8 SPEs)	2007	98.8	MI estimated by sampling	Ohara ³ [48]
Def.		Multi-rigid	MI	Simplex	FPGA (1 x Altera EP2S180 200MHz)	2007	13.4	MI fully computed in h/w	Dandekar ³ [51]
		B-spline	MI	Grad. desc.	QS20 (2 × Cell/BE.: 2 × 1 PPE & 8 SPEs)	2008	66.9	MI estimated by sampling	Rohrer [49]

¹ : Normalized performance in milliseconds per mega voxel per iteration (ms/MVoxel/itr). ² : Previously unpublished result. ³ : Additional information provided by the authors used to complete the table or to compute normalized performance results.

759 [9] A. Collignon, F. Maes, D. Delaere, D. Vandermeulen, P. Suetens, and G. Marchal, "Automated multimodality medical image registration using information theory," in *Proc. Int. Conf. Information Processing in Med. Imaging: Computational Imaging and Vision 3*, Apr. 1995, pp. 263–274. 822

760 823

761 824

763 [10] C. Studholme, D. L. G. Hill, and D. J. Hawkes, "An overlap invariant entropy measure of 3D medical image alignment," in *Pattern Recognit.*, 1999, vol. 32, pp. 71–86. 825

764 826

765 827

766 [11] A. Roche, G. Malandain, X. Pennec, and N. Ayache, "The correlation ratio as a new similarity measure for multimodal image registration," in *Medical Image Computing and Computer Assisted Intervention (MICCAI)*, Oct. 1998, pp. 1115–1124. 828

767 829

768 830

769 831

770 [12] W. H. Press, B. P. Flannery, S. A. Teukolsky, and W. T. Vetterling, *Numerical Recipes: The Art of Scientific Computing*, Cambridge University Press, New York, NY, USA, third edition, 2007. 832

771 833

772 834

773 [13] J. A. Nedler and R. Mead, "A simplex method for function minimization," *Computer Journal*, vol. 7, pp. 308–331, 1965. 835

774 836

775 [14] R. Shams, R. A. Kennedy, P. Sadeghi, and R. Hartley, "Gradient intensity-based registration of multi-modal images of the brain," in *Proc. IEEE Int. Conf. on Computer Vision (ICCV)*, Rio de Janeiro, Brazil, Oct. 2007. 837

776 838

777 839

778 [15] J. E. Dennis Jr and V. Torczon, "Direct search methods on parallel machines," *SIAM Journal on Optimization*, vol. 1, pp. 448–474, 1991. 840

779 841

780 [16] D. R. Jones, C. D. Pertunnen, and B. E. Stuckman, "Lipschitzian optimization without the Lipschitz constant," *J. Optim. Theory Appl.*, vol. 79, no. 1, pp. 157–181, 1993. 842

781 843

782 844

783 [17] E. Cantú-Paz, "A survey of parallel genetic algorithms," *CALCULATEURS PARALLELES*, vol. 10, 1998. 845

784 846

785 [18] T. Butz and J-P. Thiran, "Affine registration with feature space mutual information," in *Medical Image Computing and Computer Assisted Intervention (MICCAI)*, 2001, pp. 549–556. 847

786 848

787 849

788 [19] M. P. Wachowiak and T. M. Peters, "High-performance medical image registration using new optimization techniques," *IEEE Transactions on Information Technology in Biomedicine*, vol. 10, no. 2, pp. 344–353, Apr. 2006. 850

789 851

790 852

791 [20] S. Warfield, F. Jolesz, and R. Kikinis, "A high performance computing approach to the registration of medical imaging data," *Parallel Computing*, vol. 24, no. 9–10, pp. 1345–1368, Sept. 1998. 853

792 854

793 855

794 [21] C. E. Shannon, "A mathematical theory of communication," *Bell Syst. Tech. J.*, vol. 27, pp. 379–423/623–656, 1948. 856

795 857

796 [22] R. Shams and R. A. Kennedy, "Efficient histogram algorithms for NVIDIA CUDA compatible devices," in *Proc. Int. Conf. on Signal Processing and Communications Systems (ICSPCS)*, Gold Coast, Australia, Dec. 2007, pp. 418–422. 858

797 859

798 860

799 [23] *OpenMP Application Programming Interface, version 3.0*, OpenMP, <http://openmp.org/wp/openmp-specifications/>, 2009. 861

800 862

801 [24] B. Chapman, G. Jost, and R. van der Pas, *Using OpenMP: Portable Shared Memory Parallel Programming*, The MIT Press, Cambridge, Massachusetts, USA, 2008. 863

802 864

803 865

804 [25] T. Rohlfing and C. R. Maurer, Jr., "Nonrigid image registration in shared-memory multiprocessor environments with application to brains, breasts, and bees," *IEEE Trans. on Info. Technology in Biomedicine*, vol. 7, no. 1, pp. 16–25, Mar. 2003. 866

805 867

806 868

807 [26] E. Lusk W. Gropp and A. Skjellum, *Using MPI: Portable Parallel Programming with the Message Passing Interface*, MIT Press, Cambridge, MA, USA, second edition, 1999. 869

808 870

809 871

810 [27] F. Ino, K. Ooyama, and K. Hagihara, "A data distributed parallel algorithm for nonrigid image registration," *Parallel Computing*, vol. 31, no. 1, pp. 19–43, Jan. 2005. 872

811 873

812 874

813 [28] S. Ourselin, R. Stefanescu, and X. Pennec, "Robust registration of multi-modal images: Towards real-time clinical applications," in *Medical Image Computing and Computer Assisted Intervention (MICCAI)*, 2002, pp. 140–147. 875

814 876

815 877

816 [29] G. C. Sharp, N. Kandasamy, H. Singh, and M. Folkert, "GPU-based streaming architectures for fast cone-beam CT image reconstruction and demons deformable registration," *Phys. Med. Biol.*, vol. 52, no. 19, pp. 5771–5783, 2007. 878

817 879

818 880

819 [30] R. Shams and N. Barnes, "Speeding up mutual information computation using NVIDIA CUDA hardware," in *Proc. Digital Image Computing: Techniques and Applications (DICTA)*, Adelaide, Australia, Dec. 2007, pp. 555–560. 881

820 882

821 883

[31] Y. Lin and G. Medioni, "Mutual information computation and maximization using GPU," in *Proc. IEEE Computer Vision and Pattern Recognition (CVPR) Workshops*, June 2008, pp. 1–6. 884

[32] W. Plishker, O. Dandekar, S. S. Bhattacharyya, and R. Shekhar, "Towards systematic exploration of tradeoffs for medical image registration on heterogeneous platforms," in *IEEE Biomedical Circuits and Systems Conference*, Nov. 2008, pp. 53–56. 885

[33] P. Muyan-Özcelik, J. D. Owens, J. Xia, and S. S. Samant, "Fast deformable registration on the GPU: A CUDA implementation of demons," in *Proc. Int. Conf. on Computational Science and Its Applications (ICCSA)*, 2008, pp. 5–8. 886

[34] R. Shams, P. Sadeghi, R. A. Kennedy, and R. Hartley, "Parallel computation of mutual information on the GPU with application to real-time registration of 3D medical images," *submitted to Computer Methods and Programs in Biomedicine*, Apr. 2009. 887

[35] A. Ruiz, M. Ujaldon, L. Cooper, and K. Huang, "Non-rigid registration for large sets of microscopic images on graphics processors," *Journal of Signal Processing Systems*, vol. 55, no. 1–3, pp. 229–250, Apr. 2009. 888

[36] G. Soza, M. Bauer, P. Hastreiter, C. Nimsy, and G. Greiner, "Non-rigid registration with use of hardware-based 3D Bézier functions," in *Medical Image Computing and Computer Assisted Intervention (MICCAI)*, 2002, pp. 549–556. 889

[37] R. Strzodka, M. Droske, and M. Rumpf, "Image registration by a regularized gradient flow. a streaming implementation in DX9 graphics hardware," *Computing*, vol. 73, no. 4, pp. 373–389, Nov. 2004. 890

[38] A. Khamene, R. Chisu, W. Wein, N. Navab, and F. Sauer, "A novel projection based approach for medical image registration," in *Third International Workshop on Biomedical Image Registration (WBIR)*, Utrecht, The Netherlands, June 2006, pp. 247–256. 891

[39] F. Ino, J. Gomita, Y. Kawasaki, and K. Hagihara, "A GPGPU approach for accelerating 2-D/3-D rigid registration of medical images," in *Parallel and Distributed Processing and Applications*, Feb. 2006. 892

[40] C. Vetter, C. Guetter, C. Xu, and R. Westermann, "Non-rigid multi-modal registration on the GPU," in *Proc. SPIE Medical Imaging: Image Processing*, Feb. 2007. 893

[41] Z. Fan, C. Vetter, C. Guetter, D. Yu, R. Westermann, A. Kaufman, and C. Xu, "Optimized GPU implementation of learning-based non-rigid multi-modal registration," in *Proc. SPIE Medical Imaging: Image Processing*, 2008. 894

[42] N. Courty and P. Hellier, "Accelerating 3D non-rigid registration using graphics hardware," *International Journal of Image and Graphics*, vol. 8, no. 1, pp. 1–18, Jan. 2008. 895

[43] A. Kubias, F. Deinzer, T. Feldmann, S. Paulus, D. Paulus, B. Schreiber, and T. Brunner, "2D/3D image registration on the GPU," *Pattern Recognition and Image Analysis*, vol. 18, no. 3, pp. 381–389, Sept. 2008. 896

[44] *Compute Unified Device Architecture (CUDA) Programming Guide, version 2.2*, NVIDIA, <http://developer.nvidia.com/object/cuda.html>, 2009. 897

[45] *ATI stream computing user guide, version 1.4.0.a*, ATI, <http://developer.amd.com/>, 2009. 898

[46] W. Plishker, O. Dandekar, S. S. Bhattacharyya, and R. Shekhar, "Utilizing heterogeneous multiprocessing for medical image registration," *IEEE Signal Processing Mag.*, Mar. 2010. 899

[47] M. Ohara, H. Yeo, F. Savino, G. Iyengar, L. Gong, H. Inoue, H. Komatsu, V. Sheinin, and S. Daijavad, "Accelerating mutual-information-based linear registration on the Cell broadband engine processor," in *IEEE Int. Conf. on Multimedia and Expo*, 2007, pp. 272–275. 900

[48] M. Ohara, H. Yeo, F. Savino, G. Iyengar, L. Gong, H. Inoue, H. Komatsu, V. Sheinin, S. Daijavad, and Bradley Erickson, "Real-time mutual-information-based linear registration on the Cell broadband engine processor," in *IEEE Int. Symp. on Biomedical Imaging (ISBI)*, 2007, pp. 33–36. 901

[49] J. Rohrer and L. Gong, "Accelerating mutual information based 3D non-rigid registration using the Cell/B.E. processor," in *Proc. Workshop on Cell Systems and Applications (WCSA)*, 2008, pp. 32–40. 902

[50] C. R. Castro-Pareja, J. M. Jagadeesh, and R. Shekhar, "FPGA-based acceleration of mutual information calculation for real-time 3D image registration," in *Proc. SPIE Medical Imaging: Image Processing*, 2008. 903

[51] O. Dandekar and R. Shekhar, "FPGA-accelerated deformable image registration for improved target-delineation during CT-guided interventions," *IEEE Trans. on Biomedical Circuits and Systems*, vol. 1, no. 2, pp. 116–127, June 2007. 904

[52] A. Köhn, J. Drexler, F. Ritter, M. König, and H. O. Peitgen, "GPU accelerated image registration in two and three dimensions," in *Bildverarbeitung für die Medizin*, 2006, pp. 261–265. 905